physica status solidi pss a
www.pss-a.com

# An Initial Study of Ultraviolet C Optical Losses for Monolithically Integrated AlGaN Heterojunction Optoelectronic Devices

*Richard Floyd,* Kamal Hussain, Abdullah Mamun, Mikhail Gaevski, Grigory Simin, MVS Chandrashekhar, and Asif Khan*

**An initial study of losses in n-$Al_xGa_{1-x}N$ planar waveguides at $\lambda_{emission} \approx 280$ nm using monolithically integrated $Al_xGa_{1-x}N$ multiple quantum wells (MQWs)-based light-emitting diodes and detectors is presented. The epilayer structure for the integrated devices is grown on an AlN (3.5 μm thick) template over sapphire substrates. Emitter–detector optical coupling and the directional independence of radiation within the epistructure are experimentally established. A model for estimating the attenuation coefficient under these conditions is developed. The attenuation coefficient for a planar n-$Al_{0.65}Ga_{0.35}N$ waveguide is measured to be 5–6 $cm^{-1}$, and it primarily arises from the free-carrier absorption rather than surface roughness-dependent Rayleigh scattering.**

## 1. Introduction

Photonic-integrated circuits (PICs) operating in the ultraviolet C (UVC) spectrum are of interest for applications in biochemical sensing, UV Raman spectroscopy, and quantum photonics.[1–5] PICs operating in this spectral range (210–300 nm) require an active region material with a sufficiently wide bandgap to achieve the desired emission wavelength and an optically transparent waveguide stack. The ternary compound $Al_xGa_{1-x}N$ provides a tunable bandgap, allowing for its use for both the active region and waveguiding layers. Indeed, recent simulation results of $Al_xGa_{1-x}N$ layers grown over an optically thick ($t > 2$ μm) AlN spacer have revealed the promise of the AlGaN/AlN system for integrated optics.[6] To date all of the estimates of the optical attenuation of metal organic chemical vapor deposited (MOCVD) AlGaN in the deep ultraviolet spectral region have focused primarily on normal incidence transmission, typically enabled through the measurement of the optical transmission fringe contrast.[7,8] The in-plane attenuation coefficient for an n-$Al_{0.65}Ga_{0.35}N$ planar waveguide at a wavelength of $\lambda = 280$ nm has yet to be experimentally established. This fundamental parameter is a key requirement to furthering the development of III-N-based integrated optoelectronics.

This study experimentally establishes, for the first time, the total optical loss in an n-$Al_{0.65}Ga_{0.35}N$ planar waveguide. Our observed absorption lengths ≈2 mm are much greater than the 280 nm wavelength, clearly showing that PICs at this wavelength are possible. Moreover, by identifying free-carrier absorption as the fundamental contributor to the optical losses, we propose a roadmap for increasing the absorption length by reducing carrier concentration, further making these devices more practical. Examples of applications include the following: 1) planar system-on-a-chip can currently find broad application in surface gas sensing. Many common gases, e.g., acetone, have strong UV absorption lines.[9] 2) Ring resonators, such as with GaN, which has a visible–infrared absorption coefficient ranging from ≈0.1 to ≈2 $cm^{-1}$.[10,11] This is comparable with our AlGaN UVC losses reported here. Thus, using our AlGaN layers, ring resonators could be scaled into the UVC for more compact, secure PICs for data transmission.

In this article, we show the surface roughness in as-prepared AlGaN to be low enough to minimize Rayleigh scattering to a level well below free-carrier absorption. This demonstrates the practicality of UVC PICs.

For system-on-a-chip-based PICs, a low-loss waveguide is required for efficient transmission of the optical radiation from the emitter to the detector. Light-emitting diodes (LEDs) and pn-junction photodetectors are used as the emitters and detectors for these circuits. It is then crucial to develop an understanding of the multimode optical attenuation of guided UVC radiation within the waveguide stack using the integrated LED and photodetector. This is the motivation for our report here. We present our initial measurements of the optical losses for an n-$Al_{0.65}Ga_{0.35}N$ planar waveguide at $\lambda_{emission} = 280$ nm using monolithically integrated $Al_xGa_{1-x}N$ multiple quantum well (MQW) LEDs and photodetectors.

## 2. Device Structure, Fabrication, and Characterization

The epilayers for the integrated emitter and detector structures in our study were grown on AlN (≈3.5 μm thick)/basal plane

R. Floyd, K. Hussain, A. Mamun, Dr. M. Gaevski, Dr. G. Simin, Dr. MVS Chandrashekhar, Dr. A. Khan
Department of Electrical Engineering
University of South Carolina
301 Main St., Columbia, SC 29208, USA
E-mail: rsfloyd@email.sc.edu

The ORCID identification number(s) for the author(s) of this article can be found under https://doi.org/10.1002/pssa.201900801.

DOI: 10.1002/pssa.201900801

 

sapphire templates using a low-pressure custom MOCVD reactor. The structure consisted of a 1.5 μm-thick n-$Al_{0.65}Ga_{0.45}N$ contact layer ($n \approx 1–2 \times 10^{18}\,cm^{-3}$) followed by four pairs of $Al_{0.6}Ga_{0.4}N/Al_{0.4}Ga_{0.6}N$ MQWs ($\lambda_{emission} \approx 280$ nm). The p-side consisted of an electron blocking AlGaN, a polarization-doped graded composition p-AlGaN, and an Mg-doped hole-injection $p^+$-GaN cap layer ($p \approx 1 \times 10^{18}\,cm^{-3}$). Mesa-type emitter and detector devices were fabricated by first accessing the n-$Al_{0.65}Ga_{0.45}N$ via inductively coupled plasma reactive ion etching (ICP-RIE) and then making n-contacts using a Zr (150 Å)/Al (1200 Å)/Mo (350 Å)/Au (500 Å) metal stack. A 30 s 950 °C rapid thermal annealing (RTA) was used to improve the ohmic behavior and reduce the n-contact resistivity which was measured to be 6.63 Ω mm with a corresponding sheet resistance of ≈200 $\Omega\,\square^{-1}$ using standard transmission line measurement (TLM) test patterns. For the p-contact, Ni/Au was deposited followed by a 5 min 500 °C hot-plate annealing. The p-contact resistivity was measured to be $2 \times 10^{-2}\,\Omega\,cm^2$. Individual emitter and detector devices with the same epilayer structure but with active areas of ($100 \times 100\,\mu m^2$) and ($200 \times 200\,\mu m^2$) were first fabricated. The schematic cross section of these emitter/detector devices is shown in **Figure 1**a. In Figure 1b, we have plotted their emission power and responsivity as a function of wavelength. For these measurements, we used sapphire-side illumination or light collection. As can be seen from the inset in Figure 1b, at a current of 10 mA, the output power of the emitter varies nearly linearly with the pump current. The detector responsivity peaks at 1 mA $W^{-1}$ (at $\lambda = 250$ nm) and falls approximately by a factor of $10^3$ by $\lambda = 280$ nm. As can be seen from the data of Figure 1, despite their peak response wavelength difference, there is enough of an overlap in these spectra, so the same MQW epilayer structure can be used as both the emitter and detector.

Using the epilayer structure for the devices shown in Figure 1a,b, we fabricated equidistant pairs of monolithically integrated UVC emitters (100 μm × 100 μm) and detectors (200 μm × 200 μm). In **Figure 2**a, cross-sectional view of such a linear array is shown. When an emitter is forward biased, a portion of the emitted light trapped within the material was expected to be guided through the n-$Al_{0.65}Ga_{0.35}N$ layer.[6] In our experiment, this guided light leads to the generation of a photocurrent at the reverse-biased detector, confirming optical emitter–detector coupling through the n-$Al_{0.65}Ga_{0.35}N$ contact layer. To confirm that this signal was due to the guided radiation within the epistructure and not free-space transmission, we measured the signal with only the adjacent emitter forward biased. The signal was measured again after applying a UV-absorbing paint (acetone solvent, strongly absorbing at 280 nm[9]) to the mesa edge of the detector nearest to the emitter, covering the detector's sidewall. A 12 μm probe tip under 20× magnification was used to apply the paint. No change in photocurrent was experienced with and without the UV-absorbing paint, confirming the absence of free-space transmission. The UV-absorbing paint will also be on the AlGaN. As the paint has a higher refractive index than air, it would have the effect of extracting light out from the waveguide before reaching the detector, thereby leading to a lower photocurrent. However, as we did not observe a photocurrent decrease, we also preclude this possibility.

To investigate the directional dependence of the in-plane UVC radiation, we fabricated another test structure composed of a 10 × 10 array of identical devices, as shown in **Figure 3**a. In this design, the devices had a diameter of 35 μm with a center-to-center spacing of 52 μm. One of the central devices was then forward biased, and the photocurrent was measured using the surrounding array of devices in both the cardinal and oblique directions. The data of Figure 3b show the photosignal as a function of the angle with respect to the central emitter. As the detected power at any distance is independent of the propagation angle, the UVC emission radiates equally in all directions away from the emitter.

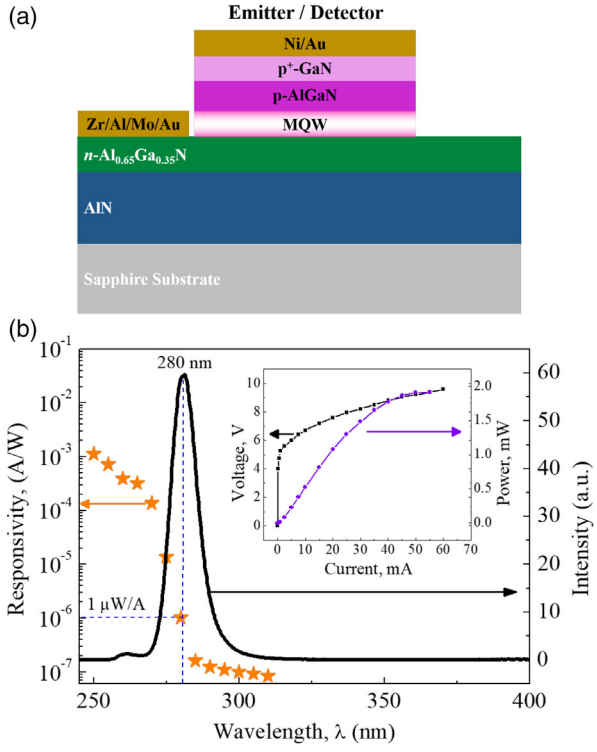


**Figure 1.** a) Device cross section. b) Standalone emitter–detector responsivity as a function of wavelength.

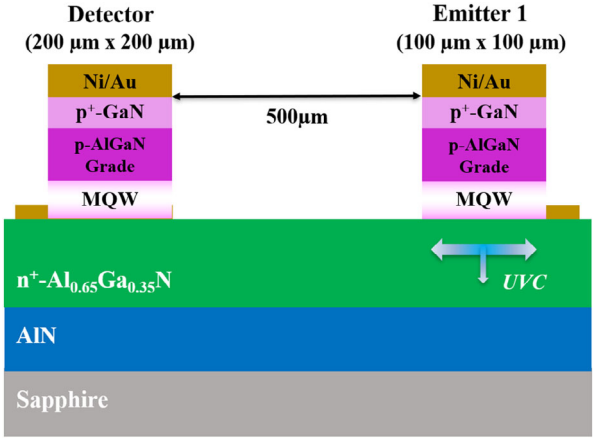


**Figure 2.** Cross-sectional view of monolithically integrated devices and the optically coupling n-$Al_{0.65}Ga_{0.35}N$ contact layer.

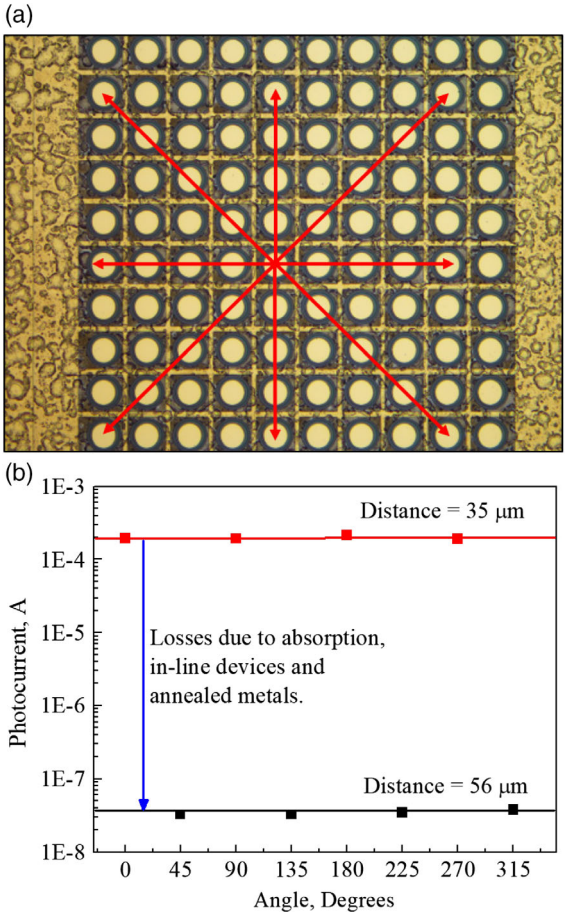


**Figure 3.** a) Top view of the central emitter surrounded by detector devices. Figure also shows the detector devices in the orthogonal (right, left, up, and down) and the oblique directions that were measured. b) Photocurrent as a function of angle between the central emitter and surrounding detector devices. The maximum difference in measured photocurrents was 15%.

## 3. n-AlGaN UVC Waveguide Losses and Attenuation Coefficient

### 3.1. Optical Loss Analysis

Combining the preferential lateral extraction of 280 nm light[12] and the directionally independent power dependence, a circular model of the propagation of light for our planar waveguide interconnects was adopted. Simulations in the literature have also predicted primarily the strongly confined propagation of UV radiation to the $Al_{0.65}Ga_{0.35}N$ epilayer using the AlGaN-on-AlN platform.[6] We then developed a simple model that would allow for the estimation of the attenuation coefficient based on the Beer–Lambert law. Approximating the emitters as point sources with the known source–detector distance, the fraction of light reaching the detector in a lossless medium can be estimated as

$$\text{Fraction of light} = \frac{\text{Detector length}}{2\pi r} \tag{1}$$

where $r$ is the source (emitter)–detector spacing, which represents the radius of the 2D circular wavefront of the guided light. Assuming a constant emitter–detector photon coupling for each emitter–detector pair yields the following proportionality for the detector photocurrent in a lossless waveguide

$$I_{\text{photo, ideal}}(\text{planar}) \propto I_{\text{pump}} \tag{2}$$

where $I_{\text{photo,ideal}}$ is the expected current at the detector and $I_{\text{pump}}$ is the emitter pump–current. The Beer's law description of light propagation intensity, $e^{(-\alpha r)}$, is now used, where $\alpha$ is the attenuation coefficient. Thus, a ratio of the measured-to-ideal photocurrent resolves to Equation (3)

$$\frac{I_{\text{photo,measured}}}{I_{\text{photo,ideal}}(\text{planar})} \propto e^{-\alpha r} \tag{3}$$

which considers the absorption of light within the material. Applying an exponential fit to Equation (3) as a function of emitter–detector spacing ($r$) on a semilog plot, we can estimate the optical attenuation coefficient of the planar waveguide.

Several mechanisms can give rise to the experienced attenuation in these planar waveguides. The mechanisms studied include Rayleigh scattering at the n-$Al_{0.65}Ga_{0.35}N$–air and n-$Al_{0.65}Ga_{0.35}N$–AlN interfaces; free-carrier-based absorption; and the intrinsic material absorption of light by the n-$Al_{0.65}Ga_{0.35}N$ waveguide layer, which is expected to be weak at $\lambda_{\text{emission}} = 280$ nm.

An early analytical model developed by Tien for estimating Rayleigh scattering losses at both the top and bottom waveguide interfaces was used to investigate its contribution to the total losses.[13] First, the surface properties of the waveguide film, $K$, were defined as

$$K = \frac{4\pi}{\lambda(\text{cm})}(\sigma_{1,2}^2 + \sigma_{1,0}^2)^{1/2} \tag{4}$$

where $\sigma_{1,2}$ and $\sigma_{1,0}$ are, respectively, the $Al_{0.65}Ga_{0.35}N$–air and $Al_{0.65}Ga_{0.35}N$–AlN interface root mean square (RMS) roughness. We can obtain the power attenuation per unit length by dividing the power lost by surface scattering, $P_{\text{ss}}$, at the two interfaces

$$P_{\text{ss}} = \frac{c}{8\pi} n_1 E_y^2 K^2 \cos^3\theta_1 \tag{5}$$

by the total power flow in the film for any waveguide mode

$$P_{\text{total}} = \frac{c}{4\pi} n_1 E_y^2 \sin(\theta_1) t_{\text{eff}} \tag{6}$$

where $c$ is the speed of light; $n_1$ is the refractive index of the waveguide medium; $E_y$ is the amplitude of the electric field; $\theta_1$ is the angle of incidence; and $t_{\text{eff}}$ is the effective thickness of the waveguiding epilayer, considering both the Goos–Hänchen shift and the layer thickness. The resulting equation for estimating attenuation due to surface roughness

$$\alpha_{\text{s}} = K^2\left(\frac{\cos^3\theta_1}{2\sin\theta_1}\right)\left(\frac{1}{t_{\text{eff}}}\right) \tag{7}$$

was simplified in this work such that the effective waveguide thickness was replaced by the actual thickness of the n-$Al_{0.65}Ga_{0.35}N$ waveguiding layer

$$\alpha_s = K^2\left(\frac{\cos^3\theta_1}{2\sin\theta_1}\right)\left(\frac{1}{t_{AlGaN}}\right) \quad (8)$$

yielding an estimation of surface-scattering losses based on the waveguide surface conditions, incident angle of light, and thickness of the waveguiding layer.

The free-carrier-based loss contribution was estimated using

$$\alpha_{fc} = \frac{Nq^3}{m_e^{*2}n\varepsilon_0\omega^2\mu_e c} \quad (9)$$

from the Drude model.[14] Here, $N$ is the free-electron concentration, $n$ is the refractive index of n-$Al_{0.65}Ga_{0.35}N$, $\omega$ is the optical frequency, $\mu_e$ is the free-electron mobility, $q$ is the elementary electron charge, $m_e$* is the effective electron mass, and $c$ is the speed of light.

### 3.2. Estimation of Losses in Our n-AlGaN UVC Planar Waveguides

We then estimated the attenuation due to Rayleigh scattering at both the top and bottom waveguide interfaces for our multimode LED emitters. The values for the ordinary and extraordinary refractive indices were taken to be 2.25 and 2.5, respectively. These values were calculated from the Sellmeier equations in the literature.[15] Using Snell's law, the critical angles for the air–AlGaN and AlGaN–AlN interfaces were determined to be 66.42° and 70.05° for trans-magnetic (TM)-polarized light. For trans-electric (TE)-polarized light, the critical angles of 63.61° and 70.43° were calculated. As these values are quite close, we used the angles associated with TM-polarized light in this estimation. The emitted light will first interact with the AlGaN–AlN interface. We then assumed that light reflected from this specular surface will propagate within the n-AlGaN waveguiding layer under the condition of total internal reflection. The geometry of our emitters permits light to enter the n-AlGaN core at a minimum angle of ≈0.06° from parallel to the interfaces. Any light with a shallower angle is not coupled from the MQWs to the n-AlGaN waveguide. The light from an LED is incoherently emitted and is multimode, making the determination of the angle(s) of incidence difficult. To account for the different incident angles, a forward travelling ray may propagate at simple boundary conditions we developed. These boundaries arose from the critical angle for total internal reflection and the minimum angle from the MQWs to the n-AlGaN core. These represent the worst- and best-case scenarios for surface scattering-induced losses. If the entirety of light propagated at the critical angle, the worst-case scattering losses were estimated to be about 2 $cm^{-1}$. If the light was all propagating at the device geometry-defined minimum angle, the scattering losses were estimated to be $3.7 \times 10^{-8}$ $cm^{-1}$. The etched n-$Al_{0.65}Ga_{0.35}N$ surface is the dominant contributor to these losses as the measured RMS roughness of the as-grown AlN is 3 times smoother.

For the contribution from free-carrier-based absorption, we used the dopant range of 1–2 × $10^{18}$ $cm^{-3}$ and calculated corresponding mobilities of 244 and 122 $cm^2$ $(V\,s)^{-1}$. The mobility was calculated from the measured sheet resistance and thickness of the n-AlGaN layer. We used the extraordinary refractive index ($n = 2.5$) and determined the effective mass of electrons to be about $0.336m_0$ based on the literature.[16] This leads to free-carrier absorption losses between 2.4 and 9.4 $cm^{-1}$.

### 3.3. Measurement of Our n-AlGaN UVC Planar Waveguide Losses

To investigate the optical losses of our planar n-$Al_{0.65}Ga_{0.35}N$ waveguides, we fabricated emitter–detector pairs with the device structures of Figure 1a. Each set of devices had varying distances between the active regions (see **Figure 4**a). The active regions of the emitter and detector were in direct line of sight. The ICP-RIE etching process used to access the n-$Al_{0.65}Ga_{0.35}N$ contact/optically coupling layer produced an RMS surface roughness of 2.5 nm, as measured by AFM.

An emitter pumping current of 10 mA was used, and the detector was reverse biased to 0.5 V. Using Equation (1)–(3) described earlier and plotting the resulting ratio of the measured to ideal photocurrent on a semilog plot, shown in Figure 4b,

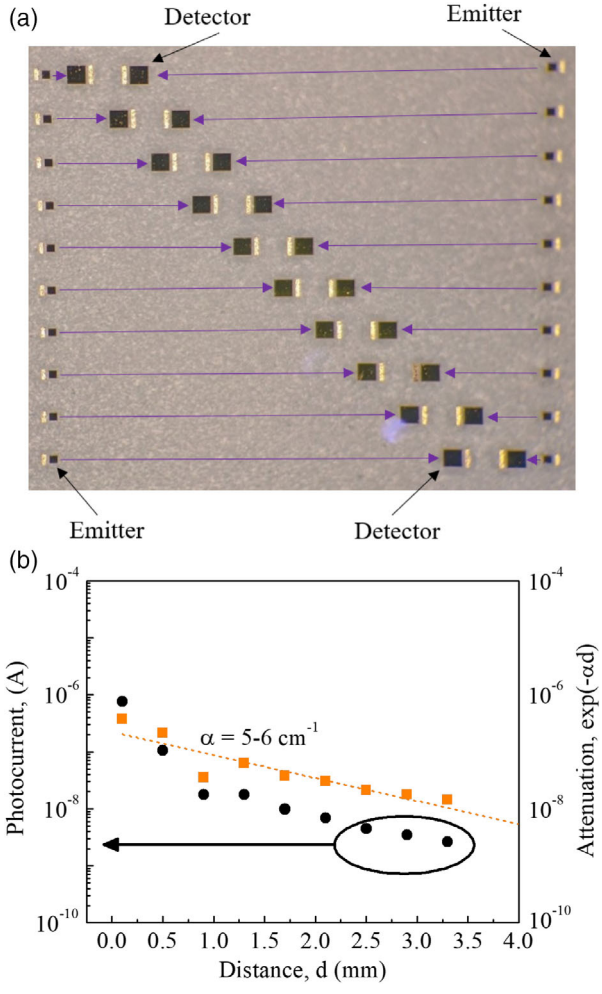


**Figure 4.** a) Micrograph image of the measured device layout. Two identical test setups are shown. b) Photocurrent (circles) and attenuation (squares) as a function of emitter–detector spacing which was varied from 100 μm to 3.7 mm.

provided an initial estimation of the overall planar waveguide attenuation coefficient. The value of the extracted attenuation coefficient was $\alpha = 5–6\ \mathrm{cm}^{-1}$ ($\approx$22–26 dB cm$^{-1}$) at $\lambda = 280$ nm. Losses of this order establish the feasibility of using AlGaN on AlN/sapphire templates for practical applications such as UV surface gas/chemical sensing as the chip dimensions are typically small.

As the dominant loss mechanism in our planar n-$Al_{0.65}Ga_{0.35}N$ waveguides appears to arise from free-carrier absorption, the use of undoped waveguiding regions should lead to a significant reduction. The roughness of etched surfaces in AlGaN can also be improved substantially by optimizing the RIE process.[17,18] We believe that these changes should decrease the losses to less than about 10 dB cm$^{-1}$ which is required for integrated optics applications such as ring resonators.[14]

We also note that these two mechanisms comprise almost the entirety of the experienced optical losses in our test structures, suggesting that intrinsic $Al_{0.65}Ga_{0.35}N$ planar waveguides may be highly transparent at UVC wavelengths.

## 4. Conclusions

In summary, we have demonstrated monolithically integrated UVC emitters and detectors coupled through an n-$Al_{0.65}Ga_{0.35}N$ waveguide. We experimentally established the directionally independent radial light propagation in the epistructure. Then, using an in-plane circular transmission model in conjunction with the Beer–Lambert law, we estimated the multimode attenuation coefficient of our n-$Al_{0.65}Ga_{0.35}N$ planar waveguide to be 2–9 cm$^{-1}$ at $\lambda_{\mathrm{emission}} = 280$ nm. This value is in good agreement with the value of 5–6 cm$^{-1}$ which was measured using only monolithically integrated emitter–detector pairs. We also show the losses to primarily arise from the Rayleigh scattering at the upper and lower waveguide interfaces and the absorption of light due to free carriers. The dominant mechanism for losses was inferred to be from free-carrier-based absorption.

## Acknowledgements

This research was supported by ARO contract W911NF-18-1-0029 monitored by Dr. M. Gerhold. Part of the AlN template work was supported by ONR MURI program monitored by Dr. Lynn Petersen and the DARPA DREAM contract (ONR N00014-18-1-2033), program manager Dr. Young-Kai Chen, monitored by Dr. Paul Maki at ONR. The sensor work was partially supported the National Science Foundation (NSF), ECCS award nos. 1711322 and 1810116, program director Dr. Dimitris Pavlidis. The authors also acknowledge the support from the University of South Carolina through the ASPIRE program.

## Conflict of Interest

The authors declare no conflict of interest.

## Keywords

AlGaN detectors, AlGaN light-emitting diodes, photonic-integrated circuits, ultraviolet C waveguides, waveguide losses

Received: September 21, 2019
Revised: December 20, 2019
Published online: January 13, 2020

[1] T. J. Lu, M. Fanto, H. Choi, P. Thomas, J. Steidle, S. Mouradian, W. Kong, D. Zhu, H. Moon, K. Berggren, J. Kim, M. Soltani, S. Preble, D. Englund, *Opt. Express* **2018**, *26*, 11147.
[2] R. Krischek, W. Wieczorek, A. Ozawa, N. Kiesel, P. Michelberger, T. Udem, H. Weinfurter, *Nat. Photonics* **2010**, *4*, 170.
[3] B. Mitra, C. Wilson, L. Que, Y. B. Gianchandani, in *Proc. of the 25th Annual Int. Conf. of the IEEE Engineering in Medicine and Biology Society*, vol. *4*, IEEE Cat. No. 03CH37439, IEEE, New York **2003**, pp. 3380–3383.
[4] W. H. P. Pernice, C. Xiong, C. Schuck, H. X. Tang, *Appl. Phys. Lett.* **2012**, *100*, 223501.
[5] H. Jung, R. Stoll, X. Guo, D. Fischer, H. X. Tang, *Optica* **2014**, *1*, 396.
[6] M. Soltani, R. Soref, T. Palacios, D. Englund, *Opt. Express* **2016**, *24*, 25415.
[7] J. F. Muth, J. D. Brown, M. A. L. Johnson, Z. Yu, R. M. Kolbas, J. W. Cook, J. F. Schetzina, *MRS Internet J. Nitride Semicond. Res.* **1999**, *4*, 502.
[8] O. Ambacher, R. Dimitrov, D. Lentz, T. Metzger, W. Rieger, M. Stutzmann, *J. Cryst. Growth* **1997**, *170*, 335.
[9] J. D. Koch, J. Gronki, R. K. Hanson, *J. Quant. Spectrosc. Radiat. Transfer* **2008**, *109*, 2037.
[10] A. Stolz, E. Cho, E. Dogheche, Y. Androussi, D. Troadec, D. Pavlidis, D. Decoster, *Appl. Phys. Lett.* **2011**, *98*, 161903.
[11] M. Gromovyi, F. Semond, J. Y. Duboz, G. Feuillet, M. P. De Micheli, *J. Eur. Opt. Soc.* **2014**, *9*, 14050.
[12] J. W. Lee, D. Y. Kim, J. H. Park, E. F. Schubert, J. Kim, J. Lee, Y. I. Kim, Y. Park, J. K. Kim, *Sci. Rep.* **2016**, *6*, 22537.
[13] P. K. Tien, *Appl. Opt.* **1971**, *10*, 2395.
[14] H. Chen, H. Fu, X. Huang, X. Zhang, T. H. Yang, J. A. Montes, I. Baranowski, Y. Zhao, *Opt. Express* **2017**, *25*, 31758.
[15] N. A. Sanford, L. H. Robins, A. V. Davydov, A. Shapiro, D. V. Tsvetkov, A. V. Dmitriev, S. Keller, U. K. Mishra, S. P. DenBaars, *J. Appl. Phys.* **2003**, *94*, 2980.
[16] S. Schöche, P. Kühne, T. Hofmann, M. Schubert, D. Nilsson, A. Kakanakova-Georgieva, E. Janzén, V. Darakchieva, *Appl. Phys. Lett.* **2013**, *103*, 212107.
[17] Y. Han, S. Xue, T. Wu, Z. Wu, W. Guo, Y. Luo, Z. Hao, C. Sun, *J. Vac. Sci. Technol. A* **2004**, *22*, 407.
[18] M. A. Miller, M. H. Crawford, A. A. Allerman, K. C. Cross, M. A. Banas, R. J. Shul, J. Stevens, K. H. A. Bogart, *J. Electron. Mater.* **2009**, *38*, 533.

 